International Journal of Multiphase Flow 35 (2009) 1036–1050

Contents lists available at ScienceDirect

International Journal of Multiphase Flow

journal homepage: www.elsevier.com/locate/ijmulflow

A multiphase model for the hydrodynamics and total dissolved gas in tailraces

Marcela Politano *, Pablo Carrica, Larry Weber

IIHR-Hydroscience and Engineering, The University of Iowa, IA 52242-1585, USA

ARTICLE INFO

Article history:
Received 7 November 2008
Received in revised form 29 May 2009
Accepted 30 June 2009
Available online 12 August 2009

Keywords:
TDG
Spillway flow
Two-phase jets
Water entrainment

ABSTRACT

Elevated supersaturation of total dissolved gas (TDG) has deleterious effects in aquatic organisms. To minimize the supersaturation of TDG at hydropower dams, spillway flow deflectors redirect spilled water horizontally forming a surface jet that prevents bubbles from plunging to depth in the stilling basin.

A major issue regarding the prediction of the hydrodynamics and TDG in tailraces is the effect of the spillway bubbly surface jets on the flow field. Surface jets cause significant changes on the flow pattern since they attract water toward the jet region, a phenomenon called water entrainment. Bubbles create interfacial forces on the liquid, reduce the effective density and viscosity, and affect the liquid turbulence increasing the water entrainment. Most numerical studies on dams use standard single-phase models, which have demonstrated to fail to predict the hydrodynamics and TDG distribution. In this paper, an anisotropic two-phase flow model based on mechanistic principles capable of predicting water entrainment, gas volume fraction, bubble size and TDG concentration is presented.

Good agreement between model results and field data is found in the tailrace of Wanapum Dam. The simulations capture the measured water entrainment and TDG distribution. The effect of the bubbles on the hydrodynamics and TDG distribution is analyzed.

© 2009 Elsevier Ltd. All rights reserved.

1. Introduction

The Columbia and Snake River basins, the most productive sources of hydropower in the United States, are of great environmental interest, as they host the largest salmon population in the contiguous United States. After construction of the dams, 12 salmon and steelhead species were placed on the endangered species list act. Particularly, fish may be exposed to stresses associated with elevated total dissolved gas (TDG) created during voluntary or involuntary spills. Elevated TDG supersaturation may cause gas bubble disease (GBD) in fish. The effect of TDG supersaturation is complex and depends principally on TDG levels, exposure time, and swimming depth of the fish (Stroud et al., 1975; Weitkamp and Katz, 1980; Bouck, 1980). Bubbles may form under the skin, mouth, gills, fins, and eyeballs of affected fish (Canadian Council of Ministers of the Environment, 1999). Death has been observed after significant exposure to high levels of TDG by blockages of blood flow due to bubbles in the vascular system. State and Federal regulations establish water quality standards relative to TDG to protect aquatic organism (Picket and Harding, 2002; Picket and Herold, 2003; Picket et al., 2004; Maynard, 2008).

1.1. Hydrodynamics

The flow in the tailrace of a large hydropower dam is usually very complex. The large energy introduced by spillway flows, mostly dissipated in the stilling basin and adjoining tailwater channel, introduces massive amounts of bubbles and creates energetic waves and sprays. If bubbles reach deep regions into the stilling basin by direct plunging or turbulent transport, they may dissolve air into the water increasing the TDG concentration in the tailrace. In deep regions, the bubbles size distribution change due both to dissolution and to compression.

In an effort to minimize the supersaturation of dissolved gases, spillway flow deflectors have been installed in several dams. As shown in Fig. 1, deflectors redirect spilled water horizontally forming a surface jet that prevents the bubbles from plunging to depth in the stilling basin, thus reducing the air dissolution. It is observed that surface jets attract water toward the jet region, a phenomenon called water entrainment. Turan et al. (2007) described the main mechanisms causing water entrainment as acceleration of the surrounding fluid as the jets decelerates, surface currents, Coanda effect and the presence of bubbles.

Wanapum Dam is located at river mile 415.8 on the Mid-Columbia River in the state of Washington, USA. It includes 12 spillway bays and 10 generating units (Fig. 2). Field-scale observations and measurements previous to the installation of the flow deflectors in Wanapum Dam showed little water entrainment from the powerhouse to the spillway. After deflector installation,

* Corresponding author. Addreess: IIHR-Hydroscience and Engineering, The University of Iowa, 300 S. Riverside Drive, Iowa City, IA 52242-1585, USA. Tel.: +1 319 335 6393; fax: +1 319 335 5238.
E-mail address: marcela-politano@uiowa.edu (M. Politano).

0301-9322/$ - see front matter © 2009 Elsevier Ltd. All rights reserved.
doi:10.1016/j.ijmultiphaseflow.2009.06.009

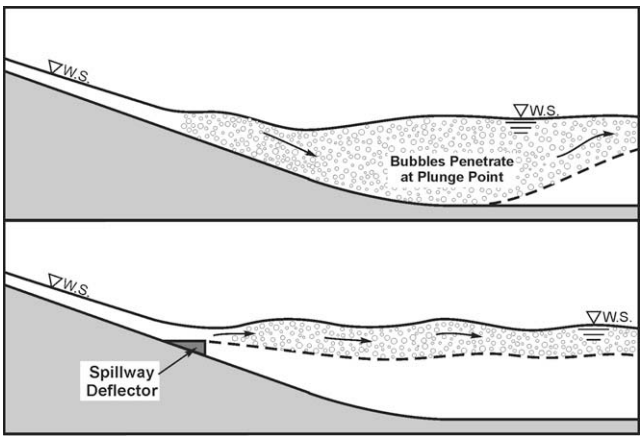

Fig. 1. Schematic of the surface jet caused by the spillway deflector.

entrainment increased very significantly, completely modifying the flow pattern in the tailrace. This flow pattern change in the tailrace affects fish passages performance, sedimentation processes, and TDG distribution, among others effects. Water entrainment due to single-phase surface jets has been subject of basic studies, though not in the context of spillway flows (Liepmann, 1990; Walker and Chen, 1994; Walker, 1997).

Numerical studies and field and model observations indicate that the presence of bubbles has a strong effect on the water entrainment. Bubbles reduce the effective density (and pressure), viscosity, and affect the liquid turbulence.

Model-scale experiments, which are scaled with the Froude number, fail to reproduce the entrainment observed in the prototype, thus preventing flow studies under some spillway operational conditions (Haug and Weber, 2006). Notice that since the scaling is performed based on the Froude number, the Reynolds and Weber numbers are not honored, resulting in smaller levels of turbulence and less and bigger bubbles (in dimensionless terms) than in the prototype. As a consequence, the bubble residence time is much shorter and the gas volume fractions much smaller, resulting in a rather ineffectual two-phase flow. This, along with inadequate representation of the turbulence, leads to much weaker surface jets and less entrainment for the model.

The prediction of the water entrainment in tailraces has received a vast amount of attention in the past. Earlier studies aimed at the prediction of the hydrodynamics in hydropower tailraces grossly underpredicted the water entrainment (Li and Weber, 2006). Turan et al. (2007) used an anisotropic mixture model that accounts for the gas volume fraction and attenuation of normal fluctuations at the free surface. Although this model predicted considerably more water entrainment than the standard isotropic single-phase models, the degree of the entrainment obtained on prototype scale was still underpredicted.

1.2. TDG

Numerical modeling can be very useful to understand the underlying phenomena leading to TDG supersaturation. The TDG concentration depends on extremely complex processes such as air entrainment in the spillway (pre-entrainment), entrainment when the jet impacts the tailwater pool, breakup and coalescence of entrained bubbles, mass transfer between bubbles and water, degasification at the free surface, and bubble and TDG transport. In addition, tailrace flows in the region near the spillway cannot be assumed to have a flat air/water interface, requiring the

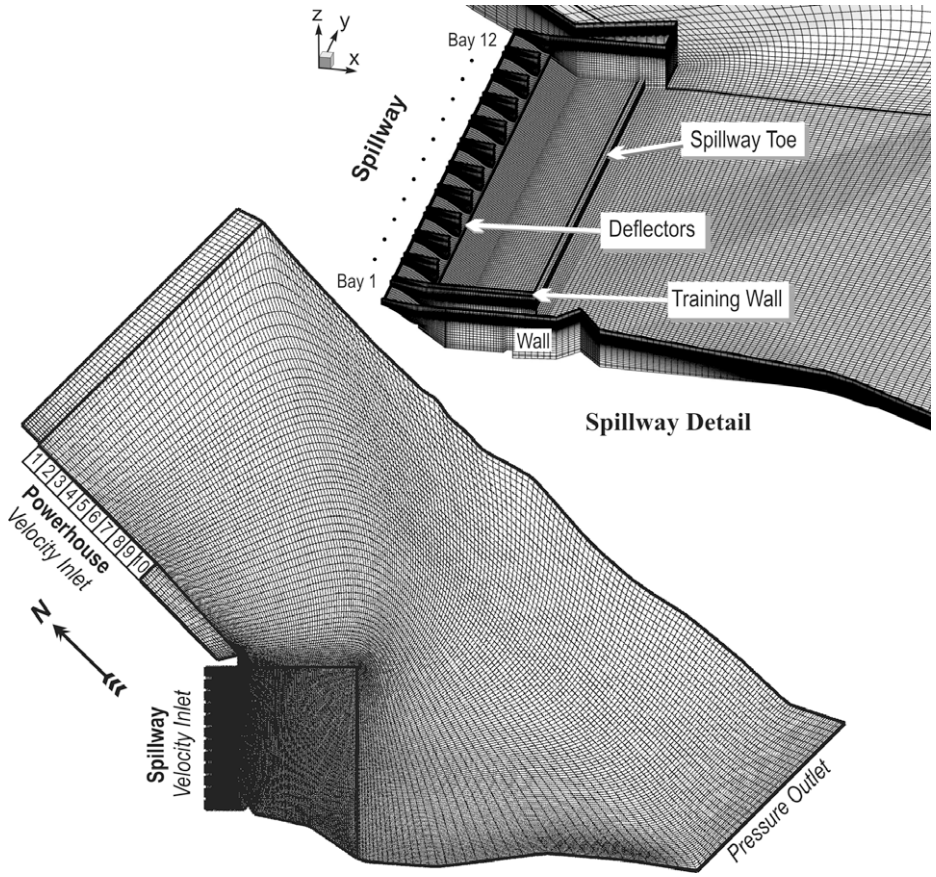

Fig. 2. Main structures and grid for the VOF Wanapum Dam model.

computation of the free surface shape. Water entrainment, discussed in the previous section, leads to mixing modifying the TDG field.

Earlier studies to predict TDG downstream of spillways were based on experimental programs (Hibbs and Gulliver, 1997; Orlins and Gulliver, 2000). This approach has been reasonably effective, though it can be very expensive and time-consuming. The most important source for TDG is the gas transferred from the bubbles, therefore a proper model for TDG prediction must account for the two-phase flow in the stilling basin and the mass transfer between bubbles and water. In addition, the model has to capture the water entrainment to correctly predict the TDG dilution due to powerhouse flows.

Free surface numerical models can predict the shape and evolution of the free surface and, though expensive, is today feasible to apply them to complex 3D flows. In the field of hydraulic engineering, free surface models are not yet widely applied but steadily developed (Turan et al., 2008; Ferrari et al., 2009). However, direct simulation of individual bubbles in a spillway/tailrace environment is well beyond current computer capabilities. Therefore, a two-phase flow model with space–time averaged quantities that does not resolve the interface is needed to model the effect of the bubbles on the flow field and bubble dissolution. Jakobsen et al. (2005) provide a complete review of the state of the art of two-phase flow modeling. Two-phase flow models using averaged quantities have been extensively used, mainly in the chemical and nuclear engineering communities, to simulate homogeneous tanks, bubble columns or vertical pipes. The first effort to incorporate a two-phase flow model to predict TDG at hydropower tailraces was carried out by Politano et al. (2007). The authors used a two-fluid model to predict the gas and TDG distribution in a 2D cross-section passing through a spillway bay. The model was compared against TDG field data measured before deflector installation and also used to study the effect of the bubble size on TDG concentration. In a later study, Urban et al. (2008) used a 1D two-phase flow equation to predict TDG in the tailrace of Ice Harbor Dam. The authors solved a TDG equation for three distinct regions of flow using a series of control volumes. Though this model takes into account the mass transfer between bubbles and the liquid phase, the model does not solve the hydrodynamics and uses several empirical correlations to calculate the eddy length scales and interfacial areas. Note that the water entrainment caused by deflectors cannot be captured with 1D or 2D simulations and consequently the TDG dilution due to powerhouse flows is not taken into account with these models. The difficulties associated with computation of large-scale flow fields have delayed the use of two-phase models to solve highly complex 3D flows. One example of a comprehensive (and expensive) two-phase polydisperse flow model was developed by Carrica et al. (1999) to predict the flow around a surface ship.

1.3. Objectives and overview

The primary goal of this study is to develop an unsteady 3D two-phase flow model capable of predicting the hydrodynamics, including the water entrainment from the powerhouse into the spillway region, and TDG distribution within hydropower tailraces. The model uses a Reynolds Stress Model (RSM) to provide anisotropic closure for the two-phase RANS equations, and introduces a simple but effective boundary condition to enforce zero normal fluctuations at the free surface. A modified bubble-induced turbulence term is added to the Reynolds stress components to account for suppression and production of turbulence by the bubbles. The TDG is calculated with a two-phase transport equation in which the source is the bubble/liquid mass transfer, function of the gas volume fraction and bubble size. Attention is focused on the effect of the bubbles on the turbulence field and water entrainment. The model is implemented into the commercial CFD code FLUENT using User Defined Functions (UDFs) and User Defined Scalars (UDSs). The numerical results are compared against field data for Wanapum Dam under two operational conditions.

2. Mathematical modeling

Any attempt to predict the water entrainment in tailraces has to include a two-way coupled approach. The presence of bubbles modifies the effective density and viscosity, and creates forces on the liquid phase due to the non-zero slip velocity. In this study, an algebraic slip mixture model (Manninen et al., 1996) that accounts for buoyancy, pressure, drag and turbulent dispersion forces is used to calculate the gas volume fraction and velocity of the bubbles.

2.1. The algebraic slip mixture model (ASMM)

The ASMM model is a simplified two-fluid model that solves continuity and momentum equations for the mixture phase and a volume fraction equation for the discrete phase. The model assumes that the gas phase is in quasi-steady state determined by local conditions. In this method the gas–liquid relative velocity is calculated with algebraic equations, after neglecting inertia, viscous and virtual mass terms usually present in a two-fluid model. Standard isotropic or anisotropic models are used to represent the mixture turbulence.

2.1.1. Mass and momentum conservation for the mixture phase

The two fluid model provides mass and momentum equations for the liquid and gas phases (Drew and Passman, 1998). Adding the mass and momentum equations for each phase results in continuity and momentum equations for the gas–liquid mixture:

$$\frac{\partial \rho_m}{\partial t} + \nabla \cdot [\rho_m \vec{u}_m] = 0 \tag{1}$$

$$\frac{\partial}{\partial t}(\rho_m \vec{u}_m) + \nabla \cdot (\rho_m \vec{u}_m \vec{u}_m) = -\nabla P + \nabla \cdot \left[\boldsymbol{\sigma}_m^{\mathrm{Re}} + \boldsymbol{\tau}_m\right] + \rho_m \vec{g} - \nabla \cdot \left(\sum_{k=g,l} \alpha_k \rho_k \vec{u}_k \vec{u}_{dr,k}\right) \tag{2}$$

where P is the total pressure, $\vec{g}$ is the gravity acceleration, and $\boldsymbol{\sigma}_m^{\mathrm{Re}}$ and $\boldsymbol{\tau}_m = \rho_m \nu_m (\nabla \vec{u}_m + \nabla \vec{u}_m^T)$ are the turbulent and molecular shear stresses, respectively. ρ_m, μ_m and $\vec{u}_m$ are the mixture density, viscosity and mass-averaged velocity defined as $\rho_m = \sum_{k=g,l} \alpha_k \rho_k$, $\mu_m = \sum_{k=g,l} \alpha_k \mu_g$ and $\vec{u}_m = \frac{1}{\rho_m} \sum_{k=g,l} \alpha_k \rho_k \vec{u}_k$, with α_g the gas volume fraction. The subscripts g, l and m denote gas, liquid and mixture, respectively. $\vec{u}_{dr,k}$ is the drift velocity defined as the velocity of the phase k relative to the mixture velocity.

The gas density is calculated using the ideal gas law $\rho_g = MP/(RT)$ with M the molecular weight of air, R the universal gas constant, and T the absolute temperature.

2.1.2. Mass conservation for the gas phase

The continuity equation for the gas phase is (Drew and Passman, 1998):

$$\frac{\partial}{\partial t}(\alpha_g \rho_g) + \nabla \cdot (\alpha_g \rho_g U_g) = -S \tag{3}$$

where $\bar{u}_g$ is the bubble velocity and S represents the bubble-liquid mass transfer.

2.1.3. Momentum conservation for the gas phase

The momentum equation of the gas phase assuming that the inertia and viscous shear stresses are negligible compared to pressure, body forces and interfacial forces results in (Antal et al., 1991; Lopez de Bertodano et al., 1994; Manninen et al., 1996):

$$0 = -\alpha_g \nabla P + \alpha_g \rho_g \vec{g} + \vec{M}_g \tag{4}$$

where $\vec{M}_g$ represents the interfacial momentum transfer between the phases. Eq. (4) is generally valid when the Stokes number defined as the ratio of the particle relaxation time to the carrier flow characteristic time is much smaller than one.

2.1.4. Bubble number density transport equation

Most of the two-phase flow models available in commercial codes (Fluent, CFX, CFDLib, among others) assume a mean constant bubble size with a given relative velocity (Chen et al., 2005). In tailrace flows the use of a mean constant bubble size for the evaluation of the bubble-liquid mass transfer and interfacial forces is not valid. This study assumes that in the region downstream of the jet impingement bubble size changes mainly due to mass transfer and pressure variations and therefore bubble breakup and coalescence processes can be neglected. This assumption is very strong, and will be the subject of future research. Breakup and coalescence are expected to be very strong at the jet impingement region, and along the spillway face. No significant breakup is expected to occur in the near region downstream of the spillway, since turbulence dissipation decreases rapidly and with it the main kernel of bubble breakup (Carrica et al., 1999). Coalescence can, however, be important anywhere where the gas volume fraction is large and the collision probability is not negligible (Politano et al., 2003a).

Let $f\,dm\,d\vec{r}$ represent the number of bubbles with mass within dm of m, located within $d\vec{r}$ of $\vec{r}$ at time t. The Boltzmann transport equation for f is:

$$\frac{\partial f}{\partial t} + \nabla \cdot \left[\vec{u}_g f\right] + \frac{\partial}{\partial m}\left[\frac{\partial m}{\partial t} f\right] = 0 \tag{5}$$

Integration of Eq. (5) for bubbles of all masses results in a transport equation for the bubble number density N:

$$\frac{\partial N}{\partial t} + \nabla \cdot \left[\vec{u}_g N\right] = 0 \tag{6}$$

The bubble radius is calculated from $R = [3\alpha/(4\pi N)]^{1/3}$. It is assumed that bubbles are only entrained in the spillway bays and that there are no volumetric sources of bubbles. Bubble generation from supersaturated TDG water is not expected to be important since nucleation sites in the tailrace are scarce.

2.1.5. Two-phase TDG transport equation

The TDG is calculated with a two-phase transport equation (Politano et al., 2007):

$$\frac{\partial \alpha_l C}{\partial t} + \nabla \cdot (\vec{u}_l \alpha_l C) = \nabla \cdot \left(\left(\nu_m + \frac{\nu_t}{Sc_C}\right)\alpha_l \nabla C\right) + S \tag{7}$$

where C is the TDG concentration, and ν_m and ν_t are the molecular and turbulent kinematic viscosity, respectively. In this study, a standard Schmidt number of $Sc_C = 0.7$ is used.

2.1.6. Turbulence closure

The ASMM assumes that the phases share the same turbulence field. The turbulence in the mixture phase is computed using the transport equations for a single phase but with properties and velocity of the mixture. The transport equations for the Reynolds stresses $\boldsymbol{\sigma}^{\mathrm{Re}}_{i,j} = \rho_m \overline{u'_{m,i} u'_{m,j}}$ are:

$$\frac{\partial \boldsymbol{\sigma}^{\mathrm{Re}}}{\partial t} + (\nabla \cdot \vec{u}_m)\boldsymbol{\sigma}^{\mathrm{Re}} + \vec{u}_m\left(\nabla \cdot \boldsymbol{\sigma}^{\mathrm{Re}}\right) = \nabla \cdot \left[\rho_m \frac{\nu_m^t}{\sigma_R} \nabla \boldsymbol{\sigma}^{\mathrm{Re}}\right] - \mathbf{P} + \boldsymbol{\varphi} + \boldsymbol{\varepsilon} + \mathbf{S}_{\boldsymbol{\sigma}} \tag{8}$$

where the stress production tensor is given by $\mathbf{P} = \boldsymbol{\sigma}^{\mathrm{Re}} \cdot \nabla \vec{u}_m^T + \left(\boldsymbol{\sigma}^{\mathrm{Re}} \cdot \nabla \vec{u}_m^T\right)^T$, $\boldsymbol{\varepsilon} = 2/3 \mathbf{I} \rho_m \varepsilon$ and $\sigma_R = 0.85$. The pressure–strain tensor $\boldsymbol{\varphi}$ is calculated using the models proposed by Gibson and Launder (1978) and Launder (1989). In this study, $\mathbf{S}_{\boldsymbol{\sigma}}$ represents the effect of the bubbles on the Reynolds stresses.

The transport equation for the turbulent dissipation rate reads:

$$\frac{\partial}{\partial t}(\rho_m \varepsilon) + \nabla \cdot (\rho_m \vec{u}_m \varepsilon) = \nabla \cdot \left[\rho_m \left(\nu_m + \frac{\nu_m^t}{\sigma_\varepsilon}\right)\nabla \varepsilon\right] - C_{\varepsilon 1} \rho_m \frac{1}{2} \mathrm{Tr}(\mathbf{P}) \frac{\varepsilon}{k} - C_{\varepsilon 2} \rho_m \frac{\varepsilon^2}{k} + S_\varepsilon \tag{9}$$

with $C_{\varepsilon 1} = 1.44$, $C_{\varepsilon 2} = 1.92$, and $\sigma_\varepsilon = 1$. The turbulent kinetic energy is defined as $k = \frac{1}{2\rho_m}\mathrm{Tr}(\boldsymbol{\sigma})$. The source term S_ε accounts for the effect of the bubbles on the turbulent dissipation rate. The turbulent kinematic viscosity is computed as in the k–ε models using $\nu_t = C_\mu k^2/\varepsilon$, with $C_\mu = 0.09$.

2.1.7. Constitutive equations

In order to close the model, interfacial transfer terms emerging from the relative motion between the bubbles and the continuous liquid need to be modeled. The most appropriate closure laws are still subject to debate and depend strongly on the particular problem to be studied (Jakobsen et al., 2005). In particular, the closure laws to model the two-phase flow in hydropower tailraces is, to a great extent, uncharted territory. In this study standard constitutive equations are used.

2.1.7.1. Interfacial momentum. Since in this particular application there are no significant velocity gradients or flow accelerations (in the bubble scale), most interfacial forces such as lift and virtual mass are negligible compared with drag and turbulent dispersion forces:

$$\vec{M}_g = \vec{M}_g^D + \vec{M}_g^{\mathrm{TD}} \tag{10}$$

where $\vec{M}_g^D$ and $\vec{M}_g^{\mathrm{TD}}$ are the drag and turbulent dispersion terms. The drag force can be modeled as (Ishii and Zuber, 1979):

$$\vec{M}_g^D = -\frac{3}{8} \rho_m \alpha_g \frac{C^D}{R} \vec{u}_r |\vec{u}_r| \tag{11}$$

where $\vec{u}_r$ is the relative velocity of the gas phase respect to the liquid phase. Most of the numerical studies use drag correlations based on rising bubbles through a stagnant liquid proposed by Ishii and Zuber (1979) and Tomiyama (1998):

$$C^D = \begin{cases} \max\left[\frac{24\left(1+0.15\mathrm{Re}_b^{0.687}\right)}{\mathrm{Re}_b}, \frac{8}{3}\frac{Eo}{Eo+4}\right], & \text{if} \quad N_\mu < 0.11\left(\frac{1+\psi_g}{\psi_g^{8/3}}\right) \\ \frac{4}{3} R_g \sqrt{\frac{g\Delta\rho}{\sigma}}\left\{\frac{1+17.67[g(\alpha)]^{6/7}}{18.67\, g(\alpha)}\right\}^2, & \text{if} \quad N_\mu \geqslant 0.11\left(\frac{1+\psi_g}{\psi_g^{8/3}}\right) \end{cases} \tag{12}$$

where $R_g^* = R_g\left(\frac{\rho_c g \Delta\rho}{\mu_c^2}\right)^{1/3}$, $g(\alpha) = \sqrt{1-\alpha}(\mu_c/\mu_m)$, $N_\mu = \mu_c(\rho_c \sigma \sqrt{\sigma/(g\Delta\rho)})^{-0.5}$ and $\psi_g = 0.55\left[\left(1+0.08 R_g^{*3}\right)^{4/7} - 1\right]^{0.75}$ with μ the viscosity. Subscripts c and m indicate continuous phase and mixture, respectively. Note that variables and fluid properties used to calculate Eq. (12) have dimensions. Small-scale turbulent motions affect the drag force (Lane et al., 2005). Experimental studies demonstrate that the effect of the turbulence on the drag coefficient is function of the Kolmogoroff scale, λ, and bubble diameter. For the application presented in this paper $\lambda_{\min} \sim 0.5 \times 10^{-4}$ m, and the correction of the drag coefficient due to turbulence according to the correlation proposed by Lane et al. (2005) is at most 1%, with

the maximum value occurring near the toe of the spillway. For this reason the turbulence correction of the drag coefficient is neglected in this paper.

The turbulent dispersion term is modeled as (Carrica et al., 1998):

$$\vec{M}_g^{\mathrm{TD}} = -\frac{3}{8}\frac{\nu^t}{Sc_b}\rho_m\frac{C^D}{R}|\vec{u}_r|\nabla\alpha_g \tag{13}$$

where $Sc_b = \nu^t/\nu^b$ is the bubble Schmidt number. Following Carrica et al. (1998, 1999), $Sc_b = 1$ is used.

2.1.7.2. Bubble dissolution and absorption. The rate of mass transfer is computed considering that the air is soluble in water and obeys Henry's law and that the air molar composition is that of equilibrium at atmospheric pressure, which implies that the air is considered a single gas with molar averaged properties. The mass flux from gas to liquid can be expressed by (Deckert, 1992; Politano et al., 2007):

$$S = 4\pi NR^2 k_l\left(\frac{P+\sigma/R}{H} - C\right) \tag{14}$$

where σ is the interfacial tension and H is Henry's constant. The second term on the RHS of Eq. (14) accounts for the effect of the interfacial tension on the equilibrium concentration. Takemura and Yabe (1998) proposed a correlation for the mass transfer coefficient of spherical rising bubbles, where the turbulence is generated by the bubble rising:

$$k_l^{rb} = \frac{DPe_b^{0.5}}{\sqrt{\pi R}}\left(1 - \frac{2}{3\left(1+0.09\mathrm{Re}_b^{2/3}\right)^{0.75}}\right) \tag{15}$$

where D is the molecular diffusivity and the bubble Peclet number is $Pe_b = 2|\vec{u_r}|R/D$. In turbulent flows, the mass transfer coefficient can be calculated using the expression proposed by Lamont and Scott (1970):

$$k_l^t = 0.4Sc^{-1/2}(\nu\varepsilon)^{1/4} \tag{16}$$

where $Sc = D/\nu$. In this application, the same order of magnitude is obtained from Eqs. (15) and (16), and the maximum mass transfer coefficient of bubbles rising in stagnant liquid (k_l^{rb}) or bubbles in turbulent flow (k_l^t) is used: $k_l = \max(k_l^{rb}, k_l^t)$.

2.1.7.3. Effects of bubbles on the mixture turbulence. The modeling of the interfacial terms for the turbulent transport equations has attracted considerable attention in recent years. The effect of the bubbles on the turbulent fluctuations is very complex as it depends on the bubble Reynolds number, gas volume fraction and bubble size. In general, large bubbles tend to enhance turbulence, whereas small bubbles may be expected to suppress turbulence (Gore and Crowe, 1989). A comprehensive study of available models for turbulence production was presented by Zboray and de Cachard (2005). Most two-phase flow models use an empirical expression for the bubble-induced turbulence. This approach was used by Davidson (1990), Sheng and Irons (1995), Buwa and Ranade (2002) and Politano et al. (2003b), among others. Most of the available models found in the literature are for bubble-induced turbulence (turbulence production). Model coefficients representing the fraction of bubble-induced turbulence going into the large-scale turbulence of the liquid phase were established for each particular problem. Coefficients for bubble columns in the literature vary from 0.02 to 0.9. Little literature is found regarding bubble turbulence suppression. Kataoka et al. (1993) proposed a model assuming that the turbulent absorption term is proportional to the interfacial area concentration and to the turbulent kinetic energy.

In this study, the model proposed by Kataoka et al. (1993) for the suppression and production of the kinetic turbulent energy is used. As the anisotropy is hardly affected by bubbles (Wang et al., 1987), the source term for the transport equation of a stress component is assumed to be proportional to that stress component and to the kinetic turbulent energy:

$$\mathbf{S}_{\boldsymbol{\sigma}} = \frac{\alpha}{2Rk}\left(-C_u k^{3/2} + C^D\left|\vec{u_r}\right|^3\right)\mathrm{diag}(\boldsymbol{\sigma}) \tag{17}$$

where C_u is a parameter of the model. Kataoka et al. (1993) used $C_u = 1$ to match the experimental two-phase flow data in a vertical channel. In this study, C_u is selected to match the measured water entrainment and TDG distribution. The effect of bubbles in the turbulence dissipation rate is modeled following Solbakken and Hjertager (1998):

$$S_\varepsilon = C_{\varepsilon 1}\frac{\alpha\rho_m}{2R}\left(C_u k^{3/2} + C^D\left|\vec{u_r}\right|^3\right)\frac{\varepsilon}{k} \tag{18}$$

The effect of the bubbles on the turbulence in the mixture model is accounted on the air/water mixture. The gas volume fractions used in the applications presented in this study are small, therefore it is expected similar mixture and liquid velocities, and thus comparable mixture and liquid fluctuations. Consequently, Eqs. (17) and (18) developed for the liquid turbulence in a two-fluid model are most probably appropriate for the air/water mixture. However, the range of applicability of these expressions should be confirmed by basic research in simpler flows, which is beyond the scope of this paper.

3. Numerical modeling

The model used in this study is based upon the commercial code FLUENT 6.2, which offers flexibility in the programming for specific physical models and boundary conditions.

3.1. Bubble velocity

Substituting Eqs. (10)–(13) into Eq. (4), an algebraic equation for the relative velocity $\vec{u}_r$ is obtained:

$$0 = \alpha\nabla P + \rho_g\alpha\vec{g} - \frac{3}{8}\alpha\rho_l\frac{C^D}{R}\vec{u}_r|\vec{u}_r| - \frac{3}{8}\rho_l\frac{\nu_t}{Sc_b}\frac{C^D}{R}|\vec{u}_r|\nabla\alpha \tag{19}$$

Note that Eq. (19) allows the bubbles to move at different velocities depending on their sizes.

3.2. Free surface modeling

The tracking of the interface can be accomplished in FLUENT using the VOF method, which solves the single-phase RANS equations coupled to a surface-capturing algorithm. In the VOF model, the interface between fluids is calculated with a transport equation for the water volume fraction α_w:

$$\frac{\partial\alpha_w}{\partial t} + \mathbf{v}\cdot\nabla\alpha_w = 0 \tag{20}$$

Mass conservation requires that $\alpha_w + \alpha_a = 1$. The jump conditions across the interface are embedded in the model by defining the fluid properties as: $\phi = \phi_w\alpha_w + \phi_a(1-\alpha_w)$, where ϕ is either the density or the viscosity. Note that α_w has different interpretation in the VOF and the ASSM models. In the VOF approach, each control volume contains just one phase (or the interface). Points in water have $\alpha_w = 1$, points in air have $\alpha_w = 0$, and points near the interface have $0 < \alpha_w < 1$. On the other hand, in the mixture model α_g represents the volume fraction of bubbles in a control volume and several interacting phases can be present in each control volume.

The VOF method has demonstrated to work very well for flow regime predictions (Turan et al., 2008). However, this method

underpredicts the water entrainment observed in hydropower tailraces because it does not account for the reduction of the normal fluctuations at the free surface (Turan et al., 2007). The implementation of attenuation of normal fluctuations at the free surface in a VOF approach is complex in the framework of UDFs. The enforcement of zero normal fluctuations requires the design and programming of body forces in the region near the interface. On the other hand, the computation of the free surface using the VOF model in a complex large water body as found in tailraces is computationally very time consuming. Depending on the river flowrate and operational conditions, a steady state condition is typically reached after 20–30 min (flow physical time), which corresponds to more than 2 months of CPU time with a 4-processor PC.

In this study, the VOF method is used to estimate the spillway jet regime and the free surface shape in a small domain near the spillway region, assuming that the bubble effects on the surface shape are negligible. The predicted free surface is then fixed throughout the computation (rigid, non-flat lid approach) to compute the water entrainment and TDG concentration in an extended domain. The use of a rigid lid approach allows increasing the time step by about 1000 times.

3.3. Simulation conditions

The performance of the model to predict the TDG distribution and water entrainment is evaluated using field data measured on April 27 and May 2, 2000 (USACE, 2001). Tables 1 and 2 summarize plant operation and tailwater elevation on these days. TDG measurements were obtained by the US Army Corps of Engineers for 30 stations along two transects: T1 at 244 m downstream of the spillway and T2 at 640 m downstream of the spillway (black circles in Fig. 3). In addition, instruments were incorporated on the forebay to monitor incoming TDG saturation. To complement this data, velocities were measured along three transects in the near field region of the dam (V1, V2 and V3 in Fig. 3).

According to field measurements, the water temperature is almost uniform in the tailrace. The water temperatures measured in the tailrace on April 27 and May 2, 2000, 8.5 °C and 9.5 °C, respectively, are used as model inputs.

The TDG concentration is often expressed as a percentage of the equilibrium concentration at atmospheric pressure. The equilibrium TDG concentration at atmospheric pressure and 8.5 °C and 9.5 °C are $C_\infty = 0.0152$ kg/m^3 and $C_\infty = 0.0154$ kg/m^3, respectively.

3.4. Computational mesh

The grids are generated using Gridgen V15. The geometry includes flow deflectors on all 12 spillway bays, powerhouse units, sluice gate, fish ladder and the bathymetry, and is meshed with multi-block structured grids. Grid and boundary conditions details for the VOF method are shown in Fig. 2. The VOF model boundary extends approximately 1000 m downstream of the dam. The VOF grids contain approximately 1.7×10^6 nodes. Fig. 3 shows the grid used to mesh the extended domain for the TDG computations. The TDG model includes 2000 m of the tailrace. Fig. 3b illustrates bathymetry contours of the Wanapum tailrace. The grid was based on the VOF grid. The top of the grid was extracted from the VOF computations. The refinement near the free surface, needed to minimize numerical diffusion in the VOF computations, was removed with the purpose of speeding up the TDG simulations. Grid sizes for on April 27 and May 2, 2000 are 5.8×10^5 and 6.5×10^5 grid points, respectively.

3.5. Boundary conditions

3.5.1. Free surface for the rigid-lid model

In FLUENT, the free surface using a rigid lid approach is usually modelled using symmetry boundary condition or wall with zero shear stress. The symmetry condition satisfies the kinematic and dynamic boundary conditions using zero normal gradient for all of the turbulent quantities. This condition fails to model the turbulence anisotropy caused by the free surface, which is important for this particular application. On the other hand, a zero-shear wall boundary condition uses a linear pressure–strain model to redistribute the normal stresses near the wall that has been shown to largely overpredict the attenuation of the normal fluctuations (Turan et al., 2007). In addition, symmetry and wall boundary conditions fail to model the behaviour of the gas phase and TDG at the free surface. To overcome this limitation, a boundary condition enforcing zero normal fluctuations at the free surface is implemented in Fluent. Kinematic and dynamic boundary conditions as wells as turbulence quantities are programmed through UDFs. Details of the boundary conditions used for the Reynolds stress and velocity components are found in Turan et al. (2007).

The gas phase is free to flow across the interface. Most of the studies found in the literature use a zero gradient condition for the gas velocity or assume terminal velocity at the free surface. For this particular application, these approaches result in bubble accumulation at the free surface. In this study, the normal component of the gas velocity at the free surface is calculated using a mass balance for the gas phase in each control volume contiguous to the interface and the resulting equation is implemented into FLUENT.

For the TDG concentration a Neumann boundary condition is used:

$$N_{\mathrm{TDG}} = k_l(C - C_\infty) \tag{21}$$

where N_{TDG} is the TDG flux at the free surface and k_l is the surface mass transfer coefficient. C_∞ is the TDG concentration at equilibrium (or saturation at atmospheric pressure).

For high Schmidt numbers, the mass diffusive sublayer lies entirely in the viscous sublayer and the surface mass transfer coefficient is controlled by turbulence in a thin boundary layer close to the surface (20–200 μm). Since the simultaneous measurement of

Table 1
Operational conditions at Wanapum Dam on April 27, 2000.

April 27, 2000 Tailwater elevation: 151.4 m **Spillway Discharge (m³/s)**											
1	2	3	4	5	6	7	8	9	10	11	12
169.9	339.8	339.8	339.8	339.8	337.0	342.6	342.6	337.0	339.8	339.8	339.8
Spill total: 3907.7 m³/s **Powerhouse Unit Discharge (m³/s)**											
1	2	3	4	5	6	7	8	9	10		
407.2	423.5	443.8	414.9	518.2	493.7	0.0	478.2	439.0	0.0		
Powerhouse total: 3618.5 m³/s											

Table 2
Operational conditions at Wanapum Dam on May 2, 2000.

May 2,2000 Tailwater elevation: 150.9 m **Spillway Discharge (m^3/s)**											
1	2	3	4	5	6	7	8	9	10	11	12
137.7	171.3	173.6	178.7	169.9	172.7	174.1	173.3	169.3	170.2	170.7	248.0
Spill total: 2109.7 m^3/s **Powerhouse Unit Discharge (m^3/s)**											
1	2	3	4	5	6	7	8	9	10		
433.2	430.5	447.4	436.1	444.6	489.9	0.0	430.4	450.2	0.0		
Powerhouse total: 3562.2 m^3/s											

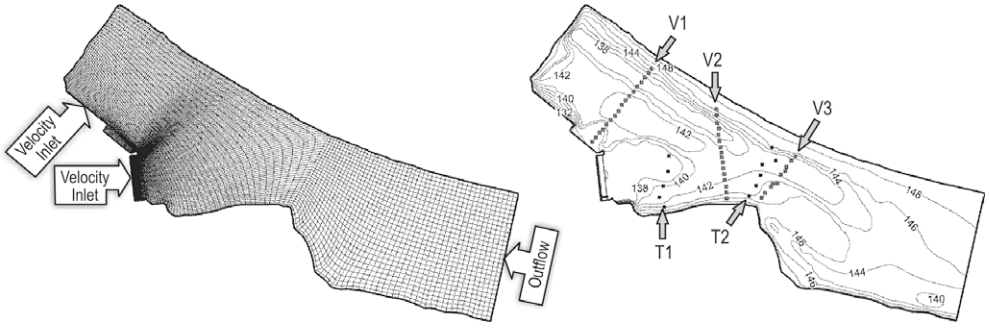

Fig. 3. Grid and boundary conditions for the TDG Wanapum Dam model.

the velocity and scalar fields in this layer is extremely difficult, the mechanism of the mass transfer is not yet well understood. Several numerical and experimental studies have been carried out to determine the mass transfer coefficient (DeMoyer et al., 2003; Calmet and Magnaudet, 1997; Stevanovik, 1998; Hasegawa and Kasagi, 2003; McKenna and McGillis, 2004; Bowyer and Woolf, 2004). Significant scatter in the experimental data and large differences between laboratory and field data were observed. In this study, a mass transfer coefficient at the free surface of $k_l = 0.0001$ m/s as measured by DeMoyer et al. (2003) for tanks and bubble columns is used.

3.5.2. Walls and river bed

The sides and the river bed are considered impermeable walls with zero TDG flux. For the gas phase, no penetration across walls is used. Previous numerical and reduced-scale models show little effect of river bed roughness on the flow field in the tailrace (Haug and Weber, 2006; Li and Weber, 2006), therefore no special treatment is used for the river bed in this study.

3.5.3. Exit

The river exit is defined as an outflow. A zero gradient condition was programmed for the TDG concentration and bubble number density.

3.5.4. Spillway bays and powerhouse units

The velocity profile predicted with the VOF method is imposed at the inlet. The air entrainment is assumed a known inlet boundary condition. Uniform velocities with constant gas volume fraction of $\alpha = 0.04$ and bubble radius $R = 0.0004$ m are used for the 12 bays in the spillway region. It must be noted that the choice of bubble size and volume fraction has an important effect on the level of entrainment. In general a bubble size distribution should be provided from experimental data. In this paper, reasonable single-size bubble diameter and volume fraction are assumed. These parameters are externally imposed inputs of the model.

It is assumed that air is not entrained with the turbine flow and that the travel time in the spillway is short so that the exposure of water to air is limited. Therefore TDG concentrations measured on April 27 and May 2, 2000 in the forebay, 116.3% and 111.4% of saturation concentration at atmospheric pressure, respectively, are used as inlet condition at the powerhouse units and spillway bays.

3.5.5. Top for the VOF simulations

A pressure outlet boundary condition with atmospheric pressure is applied at the top to allow free air flow and avoid unrealistic pressurization.

3.6. Model limitations and discussion of assumptions

In the form presented in this work, the model lacks some effects that may be important, some of which has been discussed as the different components of the formulation have been introduced. Due to the extremely complicated nature of the problem, the present model is still on a level aiming at reasonable solutions with three model parameters tuned to match known flow field and TDG distribution. In particular, the model cannot predict the bubble size and volume fraction at the input, which is an incredible difficult task if attempted numerically. The model relies on external input, hopefully obtained experimentally, of bubble probability density function and corresponding average bubble size and gas volume fraction. These measurements are possible in simpler flows, but at the impact region of a prototype spillway are extremely difficult, due to the large velocities involved (~20 m/s), the violence of the phenomenon that prevents operator proximity, and presence of debris in the water. No data is found in the literature for bubble size or void fraction in a prototype spillway. Since the process is not dimensionally scalable, model measurements are of little use. It is in the area of bubble entrainment in the near field of the plungers where significant research effort is needed to better model the two-phase flow and TDG distribution.

In addition, the breakup and coalescence of bubbles have been neglected in the model. Strong breakup and coalescence are likely to occur near the impact point. It is expected that the inclusion of the breakup and coalescence phenomena change the bubble size distribution at the plunging jet region immediately downstream

of the spillway. However, besides breakup and coalescence, the final bubble size distribution will strongly depend on the size distribution of the entrained bubbles. A polydisperse two-phase flow model, similar to those by Carrica et al. (1999) and Politano et al. (2000) to account for the evolution of the bubble size distribution is proposed as future work once two-phase flow field data are available.

Moreover, interfacial and constitutive equations for bubbly jets in the high Reynolds numbers present in a prototype spillway are scarce or inexistent in the literature, and the selection of the best models available has been performed with no certainty of their applicability for spillway flows. Improvements of these models require, again, prototype-scale experiments to provide insight of the different processes involved in the transport of bubbles and TDG, and their effect on the liquid flow field.

3.7. Solution procedure

The mixture model equations are solved sequentially with the control volume technique used by FLUENT. The VOF and rigid-lid simulations are performed using similar discretization schemes. The continuity condition is enforced using the pressure–velocity coupling SIMPLE algorithm. The pressure at the faces is calculated using the body force weighted scheme. When bubble turbulence suppression is the dominant phenomenon, an implicit treatment of the source terms is introduced to further enhance the stability of the solution. The gas volume fraction is solved using the geometric reconstruction scheme for the VOF computations and first order upwind for the mixture model.

The solution procedure is schematized in Fig. 4. Shaded blocks represent the models implemented into Fluent through UDFs. The two-phase scalar transport equations used to calculate the TDG concentration and bubble number density are implemented using UDSs.

Unsteady free surface computations are performed using variable-time step ranging from 0.001 s to 0.004 s. Typically, two to three nonlinear iterations are needed within each time step to converge all variables to a L_2 norm of the error $<10^{-3}$. The flow rate at the exit is selected as parameter to determine if the solution reaches the steady condition. A fixed-time step of 10 s is used to obtain unsteady solutions with the rigid-lid TDG model. The area weighted average TDG at the exit is selected as convergence parameter.

CFD computations are performed in a 128 processor Linux cluster with 2 GB of memory per processor.

4. Numerical results and comparison against field data

4.1. Free surface computations

The VOF model was used to investigate free surface topology for the different flow rates, headwater elevations and gates settings on May 2 and April 27, 2000. Zero velocity and turbulence are used as initial conditions in the entire domain. Surface jets are predicted in all the spillway bays due to deflectors and high tailrace elevation (about 151 m). Fig. 5 shows the evolution of the flow rate at the exit for May 2 and April 27, 2000. The horizontal line represents the target flow rate. Statistically steady solutions are obtained after approximately 30 min, which requires about 60 days of computation time. Fig. 6 shows the free surface predicted for May 2, 2000. In Fig. 6a, red and blue colors[1] represent water and air phases, respectively. The predicted free surface at external bays 1 and 12 is different due to the presence of walls. Fig. 6b shows an isosurface of $\alpha_w = 0.5$ colored by elevation representing the free surface location used to create the top of the rigid-lid grid. Note the free surface recovery downstream of the jet impingement region.

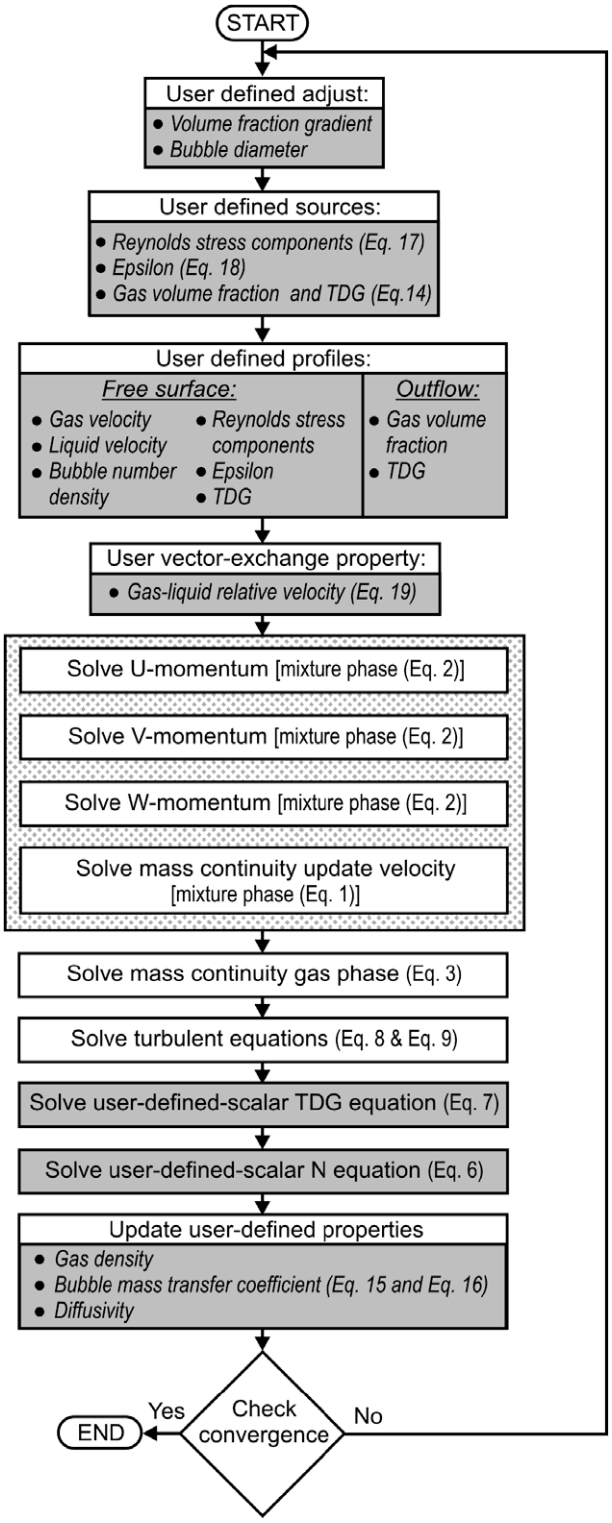

Fig. 4. Flow chart of the solution procedure.

4.2. Hydrodynamics and TDG concentration with the rigid-lid mixture model

The TDG measured at the forebay is imposed in the entire tailrace as initial condition. In order to improve convergence, the

[1] For interpretation of the references to color in Figs. 6 and 8, the reader is referred to the web version of this paper.

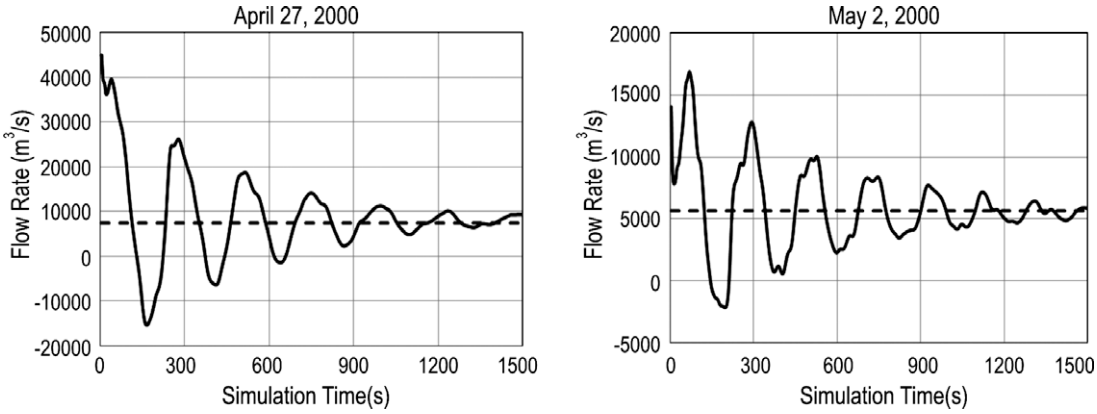

Fig. 5. Evolution of the flow rate at the exit for April 27, 2000 and May2, 2000.

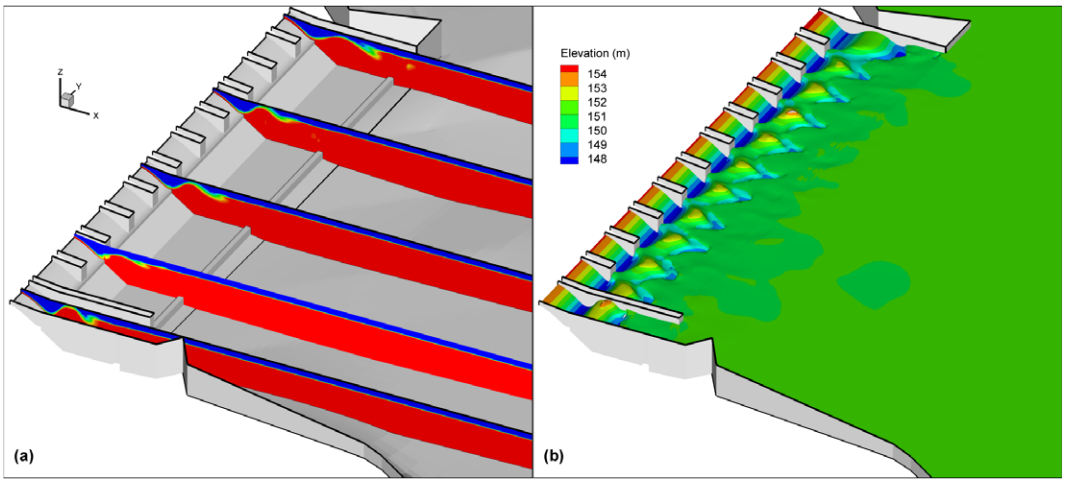

Fig. 6. (a) Gas volume fraction contours at slices passing through spillway gates. (b) Free surface colored by elevation.

model is first run as single-phase flow and then bubbles are injected in the domain. Fig. 7 shows the evolution of the area weighted average TDG at the exit for April 27, 2000 and May 2, 2000. The model requires about 4 h (7 days of wall clock computation time) to obtain a steady condition for the flow field and TDG concentration.

Fig. 8 shows velocity vectors along transects V1, V2 and V3 (see Fig. 3) on April 27, 2000 and May 2, 2000. Red and black vectors[1] represent measured and predicted data, respectively. Good agreement between observed and predicted velocity vectors is found on May 2, 2000. In order to match the field data, a bubble suppression turbulence parameter (Eq. (17)) of $C_u = 0.5$ is used.

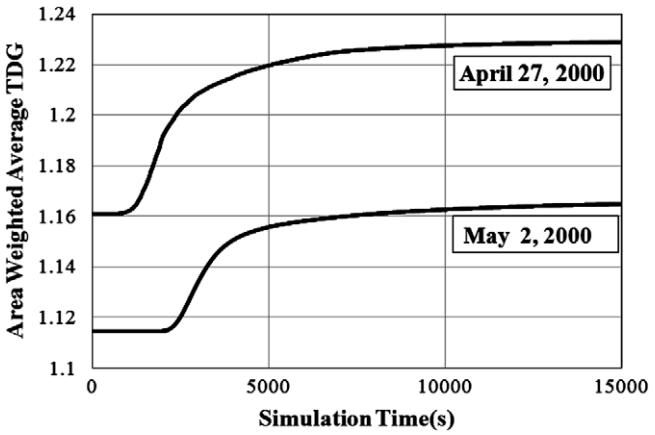

Fig. 7. Evolution of the area weighted average TDG at the exit for April 27, 2000 and May2, 2000.

Since the tailwater elevation and powerhouse flows are similar for both simulated days, the differences in the tailrace flow pattern can be mainly attributed to the different spillway flow rates. The percentage of spillway flow rates respect to the total on April 27, 2000 and May 2, 2000 were approximately 52% and 37%, respectively. Entrainment is noticed close to the west bank in the first transect (V1). In transect two (V2) more flow is observed near the west bank as a result of the water entrainment. On April 27, 2000, the model predicts a counterclockwise eddy near the east bank as a result of the strong water attraction from the powerhouse into the spillway region caused by elevated spillway flows. In the third transect (V3) the effect of the entrainment is diffused.

It must be stressed that both reduced-scale hydraulic models and standard single or two-phase models grossly underpredict the degree of entrainment observed in the field. On May 2, 2000, the predicted and laboratory measured velocity profiles along transect V2 were almost uniform (Haug and Weber, 2006; Li and Weber, 2006). As mentioned earlier, turbulence, air entrainment, and bubble size cannot be properly scaled in the hydraulic model. As surface currents originated by surface jets depend on the turbulence and the presence of bubbles, the degree of water entrainment in the hydraulic model was underestimated. Standard single-phase numerical models do not consider either the effect of the bubbles

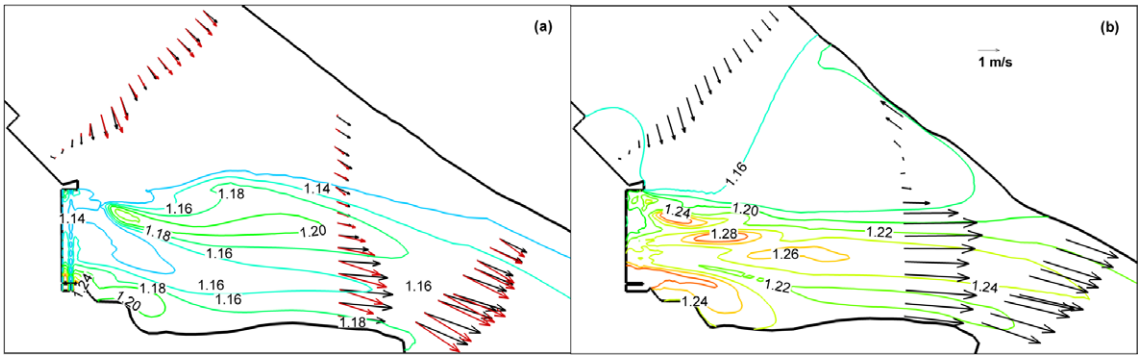

Fig. 8. Velocity vectors and TDG contours on (a) May 2, 2000 and (b) April 27, 2000.

on the flow field or the attenuation of normal fluctuations at the free surface resulting in weaker surface jets with less water entrainment. Similar results are obtained with the standard Eulerian two-phase flow model, which accounts mainly for the effect of bubbles in the turbulence field through turbulence production. On the other hand, the flow pattern in the tailrace can be captured by the present model, which includes the turbulence anisotropy at the free surface and the effect of the bubbles on the flow field.

Fig. 9 shows the TDG measured in the field at each station along transects T1 and T2 together with the values generated by the model as a function of the distance to the west shore. TDG contours at 1.5 m beneath the free surface are shown in Fig. 8. In order to match the field data a gas volume fraction of 4% and bubble diameter of 0.8 mm are used at the inlet for both simulations. The lack of measured data for these variables makes it difficult to fully validate the model. Nevertheless, model predictions agree qualitatively well with the experimental observations.

Highest TDG values were observed on April 27, 2000 due to higher spillway flow and air entrainment. The model captures the reduction of TDG with the longitudinal distance and the lateral spatial gradient observed in the field. The maximum TDG along transect T1 occurs close to the center of the spillway at about 100 m from the west shore. The TDG at the east end of the transect is diluted by flow with low TDG concentration from the powerhouse. The highest value at transect T2 is found near the west side. Notice that the concentration measured on T1 drops to 113% on May 2, 2000, and to 116% on April 27, 2000, on the east bank. On May 2, 2000, the water in this bank is coming from the powerhouse, and thus corresponds to essentially undisturbed forebay TDG concentration. On April 27, 2000, a recirculation that carries higher TDG flow from the spillway to the east bank is predicted. Note also that the model tends to overpredict TDG in this case.

Fig. 10 shows the spatial distribution of TDG and isosurfaces of TDG, gas volume fraction and bubble diameter for May 2, 2000. The highest TDG concentration is observed near the spillway endsill at the west region, reaching 140%. At this position, the powerhouse inflow is minimum. Most of the air dissolution occurs within 50–100 m downstream of the spillway, afterwards the bubbles move close to the free surface. The bubble dissolution rate decreases as the bubbles rise since the pressure is lower and bubbles are bigger. Bubble diameter isosurfaces show that bubbles shrink due to the air mass transfer and high pressure near the bed. The smaller the bubble size the stronger its tendency to dissolve. On the other side, near the free surface the bubbles grow due to the pressure drop and air absorption. Whenever the TDG concentration is higher than the saturation concentration at the local pressure, bubbles may absorb air contributing to tailrace degasification. The rate of mass exchange decreases significantly once the air bubbles disappear at the free surface. The TDG concentration reaches a developed condition approximately 1000 m from the spillway.

Fig. 11 shows streamlines colored by TDG concentration for April 27, 2000 and May 2, 2000. Water from the powerhouse entrains into the spillway region increasing its TDG level as it travels within the aerated region. It is interesting to note that the water entrainment reduces the TDG by diluting the liquid close to the powerhouse but also increases the volume of water exposed to high gas volume fraction. If bubbles are available for dissolution, the net effect of the water entrainment might be an increase of the TDG downstream. See Electronic Annexes 1 and 2 in the online version of this article for an animated version of Fig. 11.

4.3. Analysis of the effect of the bubbles on the turbulence field, water entrainment and TDG distribution

In order to match the measured TDG distribution and tailrace hydrodynamics it is necessary to include the effect of the bubbles on the turbulence field. However, the use of a turbulence constant C_u close to unity leads to overprediction of water entrainment and

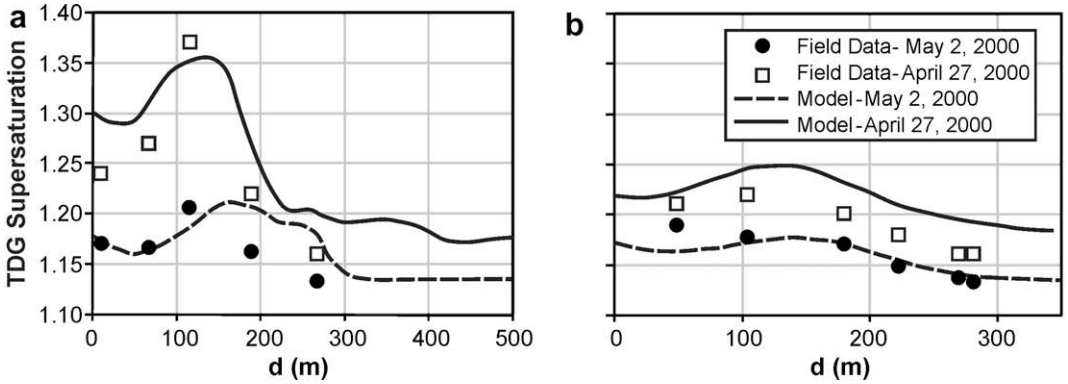

Fig. 9. TDG concentration as a function of the distance from the west shore. Symbols: measurements and lines: numerical predictions. (a) Transect 1 and (b) transect 2.

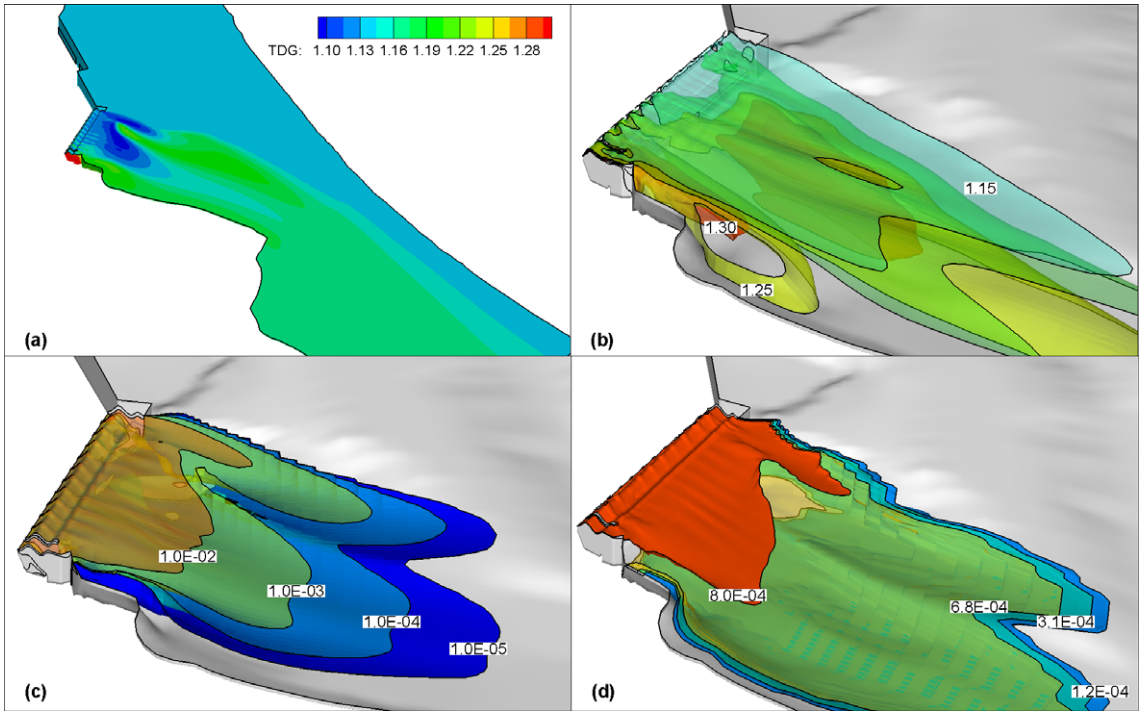

Fig. 10. Two-phase flow variables and TDG for May 2, 2000. (a) TDG contours. Isosurfaces near the spillway, (b) TDG, (c) gas volume fraction, and (d) bubble diameter.

excessive TDG dilution. The effect of the bubbles on the flow field is analyzed for May 2, 2000.

Fig. 12 shows turbulence suppression and production by the bubbles at elevations 149.5 m and 146.5 m., in the center of spillway bay 12, as a function of the longitudinal distance from the spillway toe. Black lines indicate gas volume fraction. For this particular application, the turbulence suppression is the dominant phenomenon. A peak of gas volume fraction and turbulence suppression is observed near the spillway toe because of the proximity to the free surface (Fig. 12a). The suppression of the turbulence is most significant in the first 100 m downstream of the spillway, dropping rapidly as the distance to the spillway increases, as both the volume fraction and the turbulence levels decrease. It is interesting to note that near the spillway the suppression of the turbulence is important even at deeper regions with low gas volume fractions (Fig. 12b). The maximum

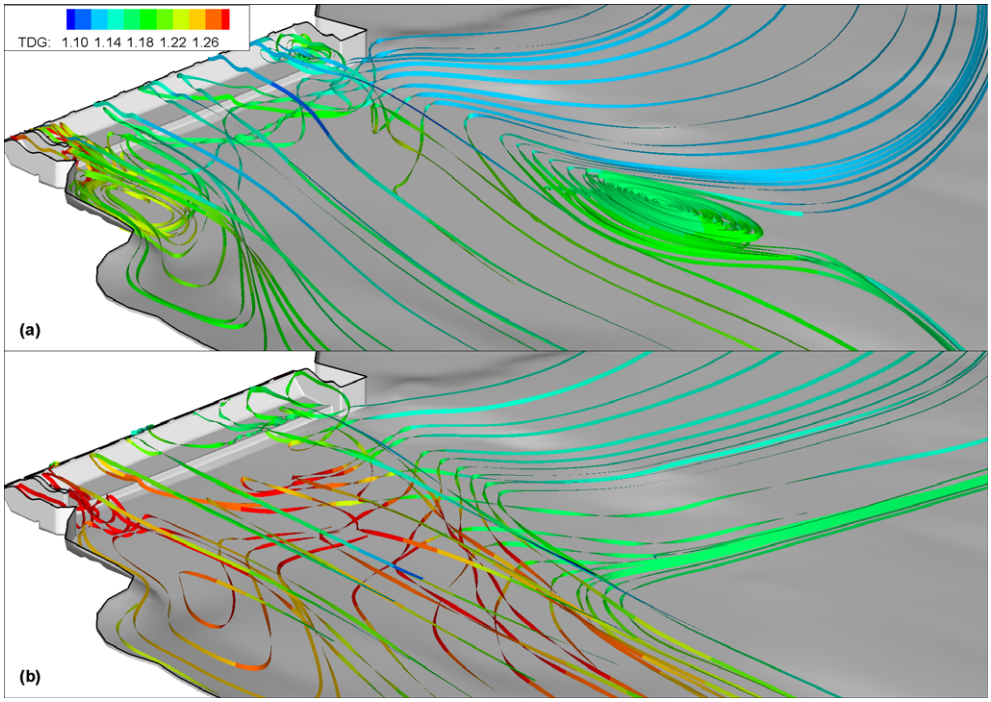

Fig. 11. Streamlines colored by TDG concentration. (a) May 2, 2000 and (b) April 27, 2000.

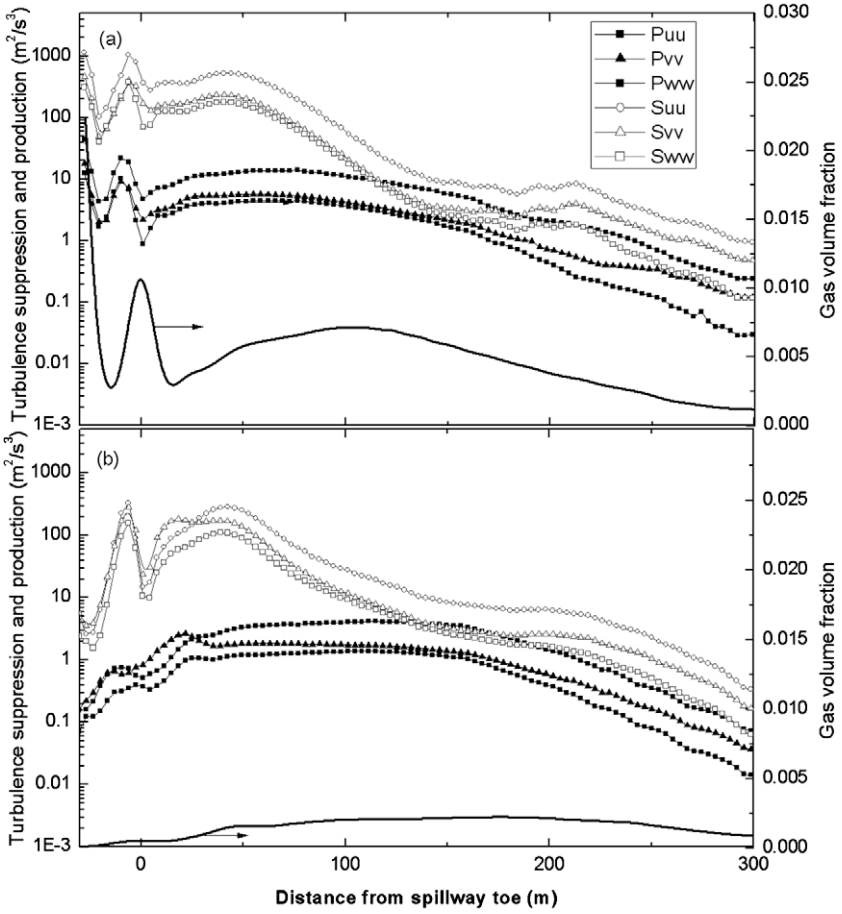

Fig. 12. Turbulence suppression and production by bubbles in the middle of spillbay 12 at (a) 1.5 m (top) and (b) 4.5 m (bottom) beneath the free surface for May 2, 2000.

bubble turbulence suppression values are due to the higher turbulence absorption by the bubbles at elevated turbulent kinetic energy. The turbulence suppression by the bubbles is partly responsible for maintaining a strong jet near the spillway, which would be rapidly dissipated with elevated levels of turbulent mixing.

Fig. 13 shows predicted velocity vectors 1.5 m beneath the free surface with and without bubble turbulence suppression. If the bubble turbulence suppression source is not included (Fig. 13a), the model is able to predict some entrainment from the powerhouse but most of entrainment is restricted to the east region of the spillway. The inclusion of the bubble turbulence suppression (Fig. 13b) causes a larger portion of the powerhouse flow attracted towards the spillway region instead of flowing toward the exit.

Fig. 14 shows isosurfaces of streamwise velocity colored by turbulent viscosity. Fig. 14a and b shows numerical predictions without and with the inclusion of suppression and production of the turbulence by the presence of bubbles, respectively. Though turbulent viscosity is not directly used in the Reynolds Stress Model closure, it provides a good indication of turbulent momentum diffusion. Again, suppression of turbulence and the consequent reduction in momentum diffusion contribute to maintain a strong surface jet and the resulting entrainment.

Fig. 15 shows velocity vectors and contours of streamwise velocity at $x = 40$, 50 and 60 m downstream of the spillway face predicted with (frames d–f) and without (frames a–c) the inclusion of the bubble sources on turbulence equations. Higher streamwise velocity is observed at all the locations if the suppression of the turbulence by the bubbles is included. Both models are able to predict surface current and streamwise vorticity, however, the current is noticeably stronger when the bubble turbulence suppression is included. It can be noted that with bubble turbulence suppression the jet remains close to the free surface. Also, due to the Coanda effect the jets are drawn toward the free surface as they are transported downstream.

Gas volume fraction contours at $x = 40$, 50 and 60 m downstream of the spillway predicted with and without the inclusion of the bubbles sources on the turbulence are shown in Fig. 16. When the bubble turbulent suppression is not included bubbles are observed near the bed for the entire stilling basin (Fig. 16a–c). As is evident in Figs. 16d–f, the suppression of the turbulence by the bubbles has reduced to zero the gas volume fraction at the bottom. Not only stronger surface jets but also surface currents prevent the bubbles to be transported to deeper regions. Turbulent suppression also causes less turbulent diffusivity and in consequence less turbulent dispersion in Eq. (13). Differences in the flow field and gas distribution due to the effect of the bubbles on the turbulence persist until approximately 120 m.

The TDG concentration in the tailrace is shown in Fig. 17. The TDG distribution is consistent with the flow structure and gas distribution. The inflow of water with low TDG from the powerhouse causes dilution and promotes mixing and redistribution of TDG. The training wall near spillway bay 1 (see spillway detail in Fig. 2) avoids water attraction toward the jet region. As a consequence, a vertical recirculation upstream of the end sill transport some bubbles to depth in the stilling basin resulting in high TDG concentrations.

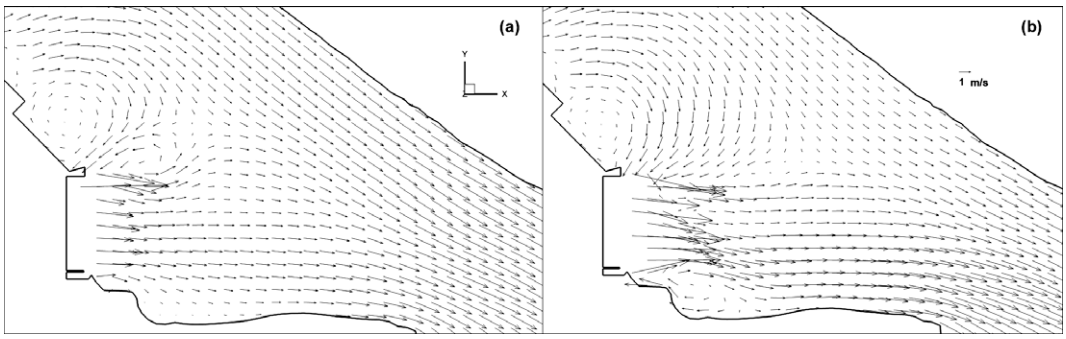

Fig. 13. Velocity vectors at 1.5 m beneath the free surface for May 2, 2000. (a) No bubble turbulence suppression and production, and (b) bubble turbulence suppression and production included.

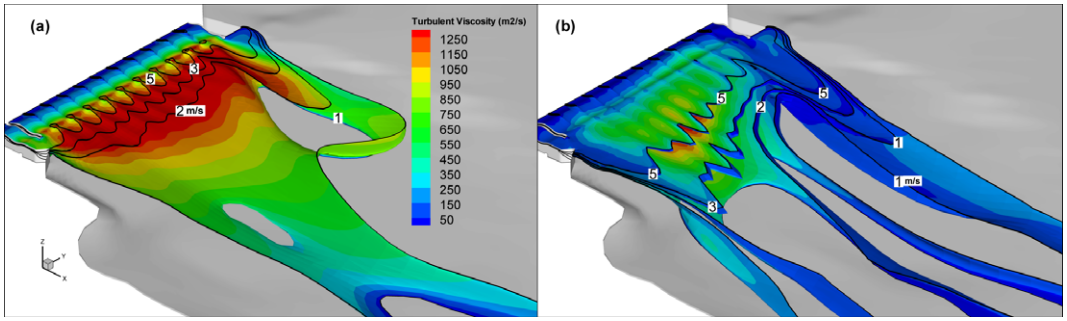

Fig. 14. Isosurfaces of streamwise velocity colored by turbulent viscosity for May 2, 2000. (a) No bubble turbulence suppression and production and (b) bubble turbulence suppression and production included. (For interpretation of the references to color in this figure legend, the reader is referred to the web version of this paper.)

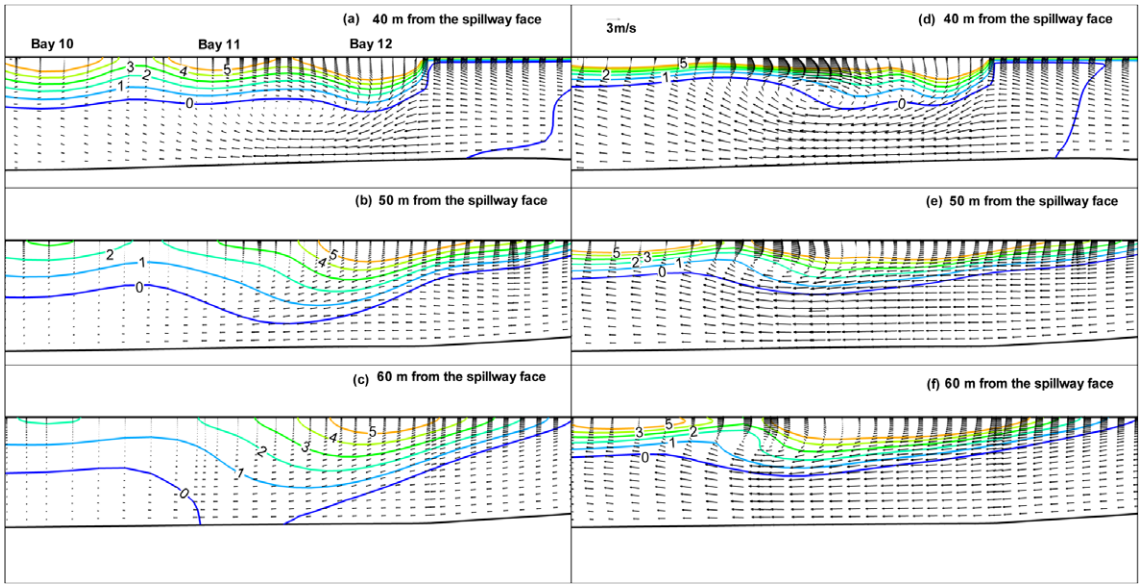

Fig. 15. Velocity vectors and streamwise velocity contours at 40 m, 50 m and 60 m downstream of spillway face for May 2, 2000. (a–c) No bubble turbulence suppression and production; and (d–f) bubble turbulence suppression and production included.

5. Conclusions and future work

A two-phase flow model aimed at the prediction of TDG is presented. The model uses an anisotropic turbulence model that accounts for bubble-induced turbulence production and suppression. To analyze dissolution and the consequent source of TDG, a variable bubble size is used. The model properly predicts the observed water entrainment from the powerhouse into the spillway, which single-phase or standard two-phase flow models are unable to predict. In addition, the predicted TDG distribution is in fairly good agreement the experimental data. The model helps to understand the different factors contributing to the production and transport of TDG in a spillway tailrace.

The results presented in this paper demonstrate that suppression of turbulence by the bubbles play a fundamental role in the prediction of the flow field and gas and TDG distribution. The inclusion of the effect of the bubbles on the turbulence field is needed to obtain the observed water entrainment caused by surface jets. It

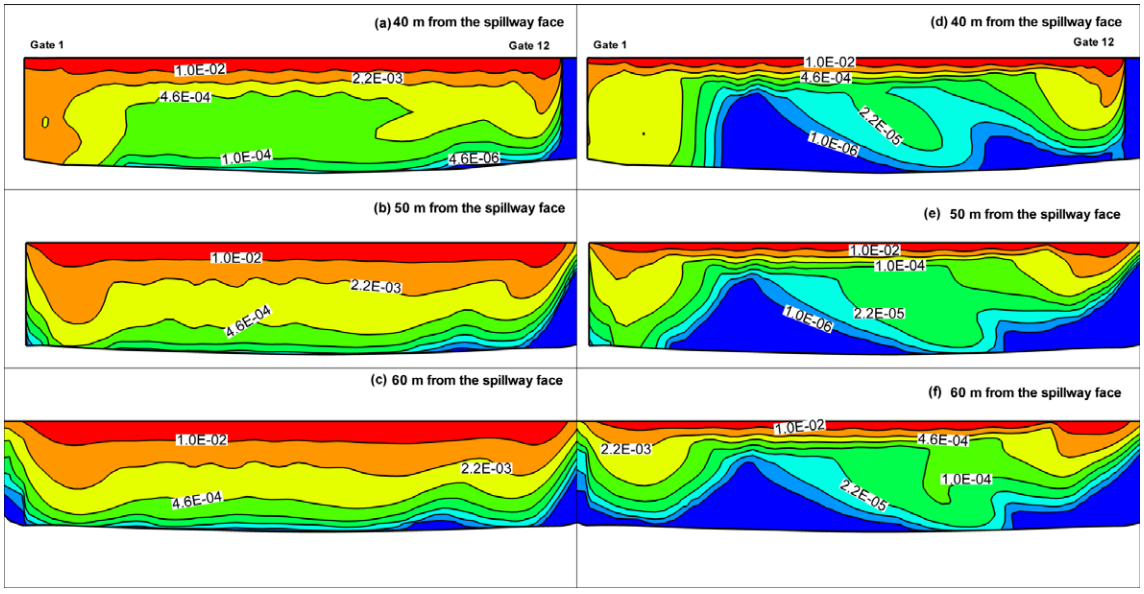

Fig. 16. Gas volume fraction contours at 40 m, 50 m and 60 m downstream of spillway face for May 2, 2000. (a–c) No bubble turbulence suppression and production; and (d–f) bubble turbulence suppression and production included.

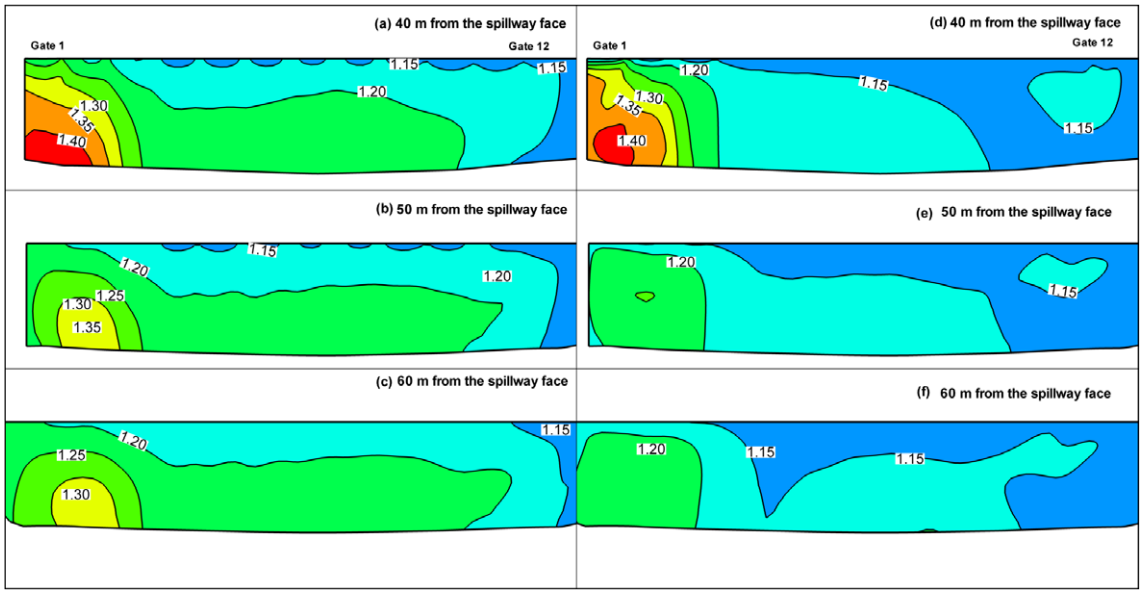

Fig. 17. TDG concentration at 40 m, 50 m and 60 m downstream of spillway face for May 2, 2000. (a–c) No bubble turbulence suppression and production; and (d–f) bubble turbulence suppression and production included.

was found that experimental data could only be matched by using a multiphase flow model with bubble turbulence suppression and an anisotropic turbulence model, which caused a slower decay in the jet strength.

The predictive capability of the presented approach is limited by the modeling accuracy of the different terms in the turbulence, bubble and TDG transport equations, the specification of the inlet conditions, and the modeling simplifications; see a discussion in the section on model limitations. The model, however, is a starting point to study the complex multiphase flow downstream of spillways and the production of TDG. A more comprehensive understanding of the range of applicability and accuracy of the models to compute the mass and momentum exchange between the phases and the effect of the bubbles in the turbulence field for highly energetic surface jets is needed. The inlet gas volume fraction and average bubble size, currently adjustable parameters to match the data, should be imposed based on experimental observations, which would remove uncertainty and allow a better evaluation of the closure models used in the formulation.

Future work includes the evaluation of the model on other dams and measurement with optical sapphire probes of bubble velocities, size distribution and gas volume fraction, tasks that will surely bring about improvements in the model. After bubble size distribution measurements are available, a multigroup approach including bubble breakup and coalescence will be implemented in the model.

Acknowledgments

The authors gratefully acknowledge the support of ANSYS, Inc.

Appendix A. Supplementary data

Supplementary data associated with this article can be found, in the online version, at doi:10.1016/j.ijmultiphaseflow.2009.06.009.

References

Antal, S.P., Lahey Jr., R.T., Flaherty, J.E., 1991. Analysis of phase distribution in fully developed laminar bubbly two-phase flow. Int. J. Multiphase Flow 17, 635–652.

Bouck, G.R., 1980. Etiology of gas bubble disease. Trans. Am. Fish. Soc. 109, 703–707.

Bowyer, P., Woolf, D., 2004. Gas exchange and bubble induced supersaturation in a wind-wave tank. Am. Meteorol. Soc. 21, 1925–1935.

Buwa, V.V., Ranade, V.V., 2002. Dynamics of gas–liquid flow in a rectangular bubble column: experiments and single/multigroup CFD simulations. Chem. Eng. Sci. 57, 4715–4736.

Calmet, I., Magnaudet, J., 1997. Large-eddy simulation of high-Schmidt number mass transfer in a turbulent channel flow. Phys. Fluids 9, 438–455.

Canadian Council of Ministers of the Environment, 1999. Canadian water quality guidelines for the protection of aquatic life: dissolved gas supersaturation. Canadian Environmental Quality Guidelines.

Carrica, P.M., Bonetto, F., Drew, D., Lahey Jr., R.T., 1998. The interaction of background ocean air bubbles with a surface ship. Int. J. Numer. Meth. Fluids 28, 528–600.

Carrica, P.M., Drew, D., Bonetto, F., Lahey Jr., R.T., 1999. A polydisperse model for bubbly two-phase flow around a surface ship. Int. J. Multiphase Flow 25, 257–305.

Chen, P., Dudukovic, M.P., Sanyal, J., 2005. Three-dimensional simulation of bubble column flows with bubble coalescence and breakup. AIChE J. 51, 696–712.

Davidson, M.R., 1990. Numerical calculations of two-phase flow in a liquid bath with bottom gas injection: the central plume. Appl. Math. Model. 14, 67–76.

Deckert, W., 1992. Bubble Column Reactors. Wiley, England.

DeMoyer, C.D., Schierholz, E.L., Gulliver, J.S., Wilhelms, S.C., 2003. Impact of bubble and free surface oxygen transfer on diffused aeration systems. Water Res. 37, 1890–1904.

Drew, D.A., Passman, S.L., 1998. Theory of Multicomponent Fluids: Applied Mathematical Sciences. Springer, New York.

Ferrari, G.E., Politano, M., Weber, L., 2009. Numerical simulations of free surface flows on a fish bypass. Comput. Fluids 338, 997–1002.

Gibson, M.M., Launder, B.E., 1978. Ground effects on pressure fluctuations in the atmospheric boundary layer. J. Fluid Mech. 86, 491–511.

Gore, R.A., Crowe, C.T., 1989. Effect of particle size on modulating turbulent intensity. Int. J. Multiphase Flow 15, 279–285.

Haug, P., Weber, L., 2006. Hydraulic model studies for fish diversion at Wanapum/Priest Rapids development-XVI: construction of 1:52 scale Wanapum tailrace model and comparison of model data with field observations. IIHR limited distribution report.

Hasegawa, Y., Kasagi, N., 2003. The role of splatting effect in high schmidt number turbulent mass transfer across an air–water interface. In: Proceedings of the Fourth International Symposium on Turbulence, Heat and Mass Transfer, vol. 4, pp. 113–120.

Hibbs, D.E., Gulliver, J.S., 1997. Prediction of effective saturation concentration at spillway plunge pools. J. Hydraul. Eng. 123, 940–949.

Ishii, M., Zuber, N., 1979. Drag coefficient and relative velocity in bubbly, droplet or particulate flows. AIChE J. 25, 843–855.

Jakobsen, H.A., Lindborg, H., Dorao, C.A., 2005. Modeling of bubble column reactors: progress and limitations. Ind. Eng. Chem. 44, 5107–5151.

Kataoka, I., Serizawa, A., Besnard, D.C., 1993. Prediction of turbulence suppression and turbulence modeling in bubbly two-phase flow. Nucl. Eng. Des. 141, 145–158.

Lamont, J.C., Scott, D.S., 1970. An eddy cell model of mass transfer into the surface of a turbulent liquid. AIChE J. 16, 513–519.

Lane, G.L., Schwarz, M.P., Evans, G.M., 2005. Numerical modeling of gas–liquid flow in stirred tanks. Chem. Eng. Sci. 60, 2203–2214.

Launder, B.E., 1989. Second-moment closure and its use in modeling turbulent industrial flows. Int. J. Numer. Meth. Fluids 9, 963–985.

Li, S., Weber, L., 2006. Comprehensive comparison of the three-dimensional computational fluid dynamics (CFD) model outputs with field data of the Wanapum Dam forebay and tailrace. IIHR limited distribution report 335.

Liepmann, D., 1990. The near-field dynamics and entrainment field of submerged and near surface jets. Ph.D. Thesis, University of California, San Diego.

Lopez de Bertodano, M.L., Lahey Jr, R.T., Jones, O.C., 1994. Development of a k–ε model for bubbly two-phase flow. J. Fluids Eng. 116, 128–134.

McKenna, S.P., McGillis, W.R., 2004. The role of free-surface turbulence and surfactants in air–water gas transfer. Int. J. Heat Mass Transfer 47, 539–553.

Manninen, M., Taivassalo, V., Kallio, S., 1996. On the mixture model for multiphase flow. VTT Publications 288, Technical Research Centre of Finland.

Maynard, C., 2008. Evaluation of total dissolved gas criteria (TDG) biological effects research: a literature review. Washington State Department of Ecology Publication Report No. 08-10-059.

Orlins, J.J., Gulliver, J.S., 2000. Dissolved gas supersaturation downstream of a spillway. II: computational model. J. Hydraul. Res. 38, 151–159.

Picket, J., Harding, R., 2002. Total maximum daily load for Lower Columbia River total dissolved gas. Report No. 02-03-004 prepared jointly by the Oregon Department of Environmental Quality and the Washington State Department of Ecology.

Picket, J., Herold, M., 2003. Total maximum daily load for total dissolved gas for Lower Snake River. Washington State Department of Ecology Publication Report No. 03-03-20.

Picket, J., Rueda, H., Herold, M., 2004. Total maximum daily load for total dissolved gas in the Mid-Columbia River and Lake Roosevelt. Submittal Report, Washington State Department of Ecology Publication No. 04-03-002.

Politano, M., Carrica, P.M., Balino, J., 2000. A polydisperse model of the two-phase flow in a bubble column. Int. J. Heat Technol. 18, 101–113.

Politano, M., Carrica, P.M., Balino, J., 2003a. About bubble breakup models to predict bubble size distributions in homogeneous flows. Chem. Eng. Commun. 190, 299–321.

Politano, M., Carrica, P.M., Converti, J., 2003b. A polydisperse two-phase model for turbulent flows in vertical channels. Int. J. Multiphase Flow 29, 1153–1182.

Politano, M.S., Carrica, P.M., Turan, C., Weber, L., 2007. A multidimensional two-phase flow model for the total dissolved gas downstream of spillways. J. Hydraul. Res. 45, 165–177.

Sheng, Y.Y., Irons, G.A., 1995. The impact of bubble dynamics on the flow in plumes of ladle water models. Metall. Mater. Trans. B 26, 625–635.

Solbakken, T., Hjertager, B.H., 1998. A computational and experimental study of flow pattern in a pilot and a full scale bubble column. In: Proceedings of the Third International Conference on Multiphase Flow, Lyon, France.

Stevanovik, V.D., 1998. An analytical model of gas absorption in open-channel flow. Proceedings of the Third International Conference on Multiphase Flow, Lyon, France.

Stroud, R.K., Bouck, G.R., Nebeker, A.V., 1975. Pathology of acute and chronic exposure of salmonid fishes to supersaturated water. In: Chemistry and Physics of Aqueous Gas Solutions, The Electrochemical Society, Princeton, NJ, USA.

Takemura, F., Yabe, A., 1998. Gas dissolution process of spherical rising gas bubbles. Chem. Eng. Sci. 53, 2691–2699.

Tomiyama, A., 1998. Struggle with computational bubble dynamics. In: Proceedings of the Third International Conference on Multiphase Flows, Lyon, France.

Turan, C., Politano, M.S., Carrica, P.M., Weber, L., 2007. Water entrainment due to spillway surface jets. Int. J. Comput. Fluid Dyn. 21, 137–153.

Turan, C., Carrica, P.M., Lyons, T., Hay, D., Weber, L., 2008. Study of a free surface flow on an ogee-crested fish bypass. J. Hydraul. Eng. 134, 1172–1175.

Urban, A.L., Gulliver, J.S., Johnson, D.W., 2008. Modelling total dissolved gas concentration downstream of spillways. J. Hydraul. Eng. 134, 550–561.

US Army Corps of Engineers (USACE), 2001. Data summary for Wanapum Dam phase 5 total dissolved gas post-deflector spillway performance test, April26–May 3, 2000. Report prepared for Public Utility District No. 2 of Grant County.

Walker, D.T., 1997. On the origin of the 'surface current' in turbulent free-surface flows. J. Fluid Mech. 339, 275–285.

Walker, D.T., Chen, C.Y., 1994. Evaluation of algebraic stress modelling in free-surface jet flows. Free Surf. Turbul. 181, 83–95. ASME.

Wang, S.K., Lee, S.J., Jones Jr, O.C., Lahey Jr, R.T., 1987. 3-D turbulence structure and phase distribution measurements in bubbly two-phase flow. Int. J. Multiphase Flow 13, 327–343.

Weitkamp, D.E., Katz, M., 1980. A review of dissolved gas supersaturation literature. Trans. Am. Fish. Soc. 109, 659–702.

Zboray, R., de Cachard, F., 2005. Simulating large-scale bubble plumes using various closure and two-phase turbulence models. Nucl. Eng. Des. 235, 867–884.